2023 IEEE International Conference on Metrology for eXtended Reality, Artificial Intelligence and Neural Engineering (MetroXRAINE) | 979-8-3503-0080-2/23/$31.00 ©2023 IEEE | DOI: 10.1109/METROXRAINE58569.2023.10405749

Cycle Aging Effect on Lithium-ion Battery Resistance: a Machine Learning Approach

Simone Barcellona
DEIB
Politecnico di Milano
Milan, Italy
simone.barcellona@polimi.it

Loris Cannelli
IDSIA Dalle Molle Institute for Artificial Intelligence
SUPSI-USI
Lugano, Switzerland
loris.cannelli@idsia.ch

Silvia Colnago
DEIB
Politecnico di Milano
Milan, Italy
silvia.colnago@polimi.it

Christian Laurano
DEIB
Politecnico di Milano
Milan, Italy
christian.laurano@polimi.it

Luigi Piegari
DEIB
Politecnico di Milano
Milan, Italy
luigi.piegari@polimi.it

***Abstract*—Nowadays, lithium-ion batteries play an important and crucial role in various applications, including electric transportation, electronic devices, medical devices, and supporting renewable energy sources. Unfortunately, they are subjected to different degradation mechanisms due to storage conditions (calendar aging) and operating conditions (cycle aging). The battery's internal resistance can be used as an indicator of its state of health. Indeed, it usually increases with aging. Moreover, the internal resistance depends on temperature and state of charge (SOC) leading to a variation law of the internal resistance with temperature and SOC. On the other hand, this variation law can change with aging. Therefore, to accurately estimate the state of health, knowledge of this dependency is required. Recently, there has been a surge in popularity and growing interest in utilizing various machine learning (ML) techniques for these purposes. In light of the above, this paper proposes a straightforward ML approach that utilizes a modest dataset with restricted features, eliminating the need for computationally demanding tools. The approach was employed and validated to estimate how the relationship between the battery's internal resistance and temperature varies with cycle aging across different SOC levels.**

Keywords—machine learning, lithium-ion battery, battery model, battery's internal resistance, battery aging

I. INTRODUCTION

Lithium-ion batteries (LiBs) are being increasingly employed in a wide range of applications, ranging from the smallest ones, such as electronic devices and medical devices to the largest ones, such as electric transportation and grid storage [1]. The energy and power exchange capabilities of LiBs depend on their internal parameters. Specifically, the battery capacity is associated with stored energy, while the battery's internal resistance is linked to its power capability.

Like other electrochemical devices, LiBs are susceptible to various degradation mechanisms caused by storage conditions (calendar aging) and operating conditions (cycle aging) [2], [3]. The former primarily depends on the state of charge (SOC) and temperature in relation to the duration of storage [4], [5]. The latter is predominantly influenced by SOC, temperature, and current rate in relation to the total charge exchanged with the battery [5], [6], [7]. The degradation affects the performance of LiBs, resulting in capacity fade (energy fade) or an increase in internal resistance (power fade). The latter will be the focus of the present work.

The estimation of the battery's internal resistance can be performed in either the time or frequency domains. Among all, the most commonly employed method is the dc current pulse, which requires injecting a current pulse into the battery under test and measuring the resulting voltage change over a specific time interval [8]. Moving to the frequency domain, electrochemical impedance spectroscopy (EIS) is one of the most widely employed methods, which consists of imposing a small sinusoidal current or voltage, at different frequencies, while measuring the corresponding (voltage or current) response [9]. This allows to evaluate the battery impedance in a wide frequency range.

The battery's internal resistance depends on the same factors that ages the battery itself. In the literature, it is possible to find many studies that evaluated the influence of SOC and temperature on the battery's internal resistance. In [10], the authors examined the internal resistance at 50% of SOC across various temperatures, establishing a mathematical relationship between internal resistance and temperature. Moreover, in [11], the correlation between internal resistance and battery capacity at different SOC and aging levels was analyzed. In [12], the influence of SOC on internal resistance was investigated, while in [13], the authors investigated the effect of calendar aging on the battery's internal resistance. Other scientists focused their attention on the effect of the cycle aging [14]. Finally, how the dependencies of internal resistance on SOC and temperature change with the battery aging were studied in [15].

In all the aforementioned works, the modeling of batteries and estimation of their parameters were conducted using analytical expressions. However, in recent years, various machine learning (ML) techniques have gained popularity and became of great interest for these purposes [16], [17].

In the present work, a simple ML approach was proposed to estimate the battery's internal resistance under different conditions of SOC, temperature, and aging levels. By utilizing a small dataset with limited features, and without the need for computationally intensive tools, the proposed solution demonstrates satisfactory estimation results in the prediction of the resistance variation in an unknown state of charge and future aging. The outcome paves the way for

979-8-3503-0080-2/23/$31.00 ©2023 IEEE

further investigation and development along the same ML direction.

II. Battery Model

In the literature, it is possible to find many different battery models that describe their electrical [18], thermal [19], or aging behavior [20]. To model the electrical behavior, the most common models are based on the circuital approach, which is particularly preferred especially in battery management systems due to their ability to provide accurate results with low computational effort [21].

Equivalent circuit models can be categorized based on their level of complexity and detail. The simplest one consists of a voltage source that models the open circuit voltage (V_{OC}) of the battery and a series resistor that models the battery's internal resistance. This model is very simple but does not allow for the investigation of the battery dynamics. One of the most comprehensive models is reported in Fig. 1. It consists of a voltage source representing the V_{OC} and, in series, the battery impedance. The latter comprises four different terms connected in series. The first term is pure ohmic resistance, R_S, which represents the electronic resistance of current collectors and electrodes, as well as the ionic resistance of electrolyte and separator. The second term is an RC parallel branch related to the solid electrolyte interface (SEI), which forms between the electrodes and electrolyte at the beginning of the battery life and continues to grow over its lifespan [22]. The third term is a parallel between the charge transfer resistance (R_{ct}), which relates to charge transfer during chemical reactions [23], and the double-layer capacity (C_d), which models the double-layer capacitance effect [21]. The last term is an element called Warburg impedance (Z_W) and models the diffusion processes into electrode/electrolyte [24].

In this paper, we focused on estimating the pure ohmic resistance, R_S.

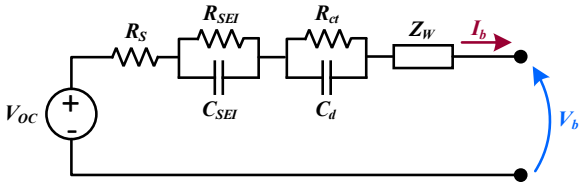

Fig. 1. Battery equivalent circuit model

The resistance R_S can be experimentally measured using several techniques, which can be divided into time-domain and frequency-domain ones. The formers are generally performed by injecting a current pulse and measuring the initial voltage drop. The latter are generally performed through the galvanostatic EIS (GEIS) where a sinusoidal current is injected at different frequencies, and the resulting impedance spectrum is analyzed. From the spectrum, the ohmic resistance can be derived simply as the value of the real part of the impedance when the imaginary part is zero. Fig. 2 presents an impedance spectrum obtained experimentally using GEIS, with the highlighted value of R_S.

III. Experimental Activity

For this analysis, the same dataset used in [15] was employed. The battery cell under test was a $LiCoO_2$ cell, which parameters are summarized in Table I.

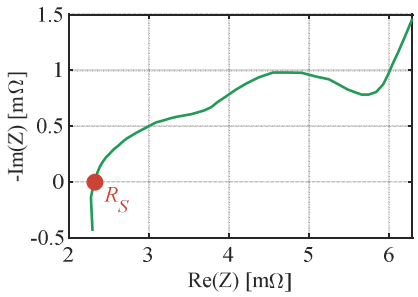

Fig. 2. Experimental GEIS

TABLE I. Cell Parameters

Parameter	Value [Units]
Rated capacity	10 [Ah]
Charge cut-off voltage	4.2 [V]
Discharge cut-off voltage	2.75 [V]
Maximum continuous discharge current	100 [A]
Maximum discharge current	150 [A]
Temperature range	(-20, +60) [°C]
Life cycles with 100% of Depth of Discharge	>300

The experimental setup is shown in Fig. 3 and consisted of a booster (VMP3B-100) connected to a potentiostat (SP-150), both from Biologic Science Instruments, controlled by a PC with ECLAB software. To control the battery temperature, three Peltier cells connected in series were placed under the battery cell. The control of the Peltier cells was performed using a Texas Instrument microcontroller (F28069M) combined with an inverter (DRV8323RX). The block diagram of the test setup is reported in Fig. 4.

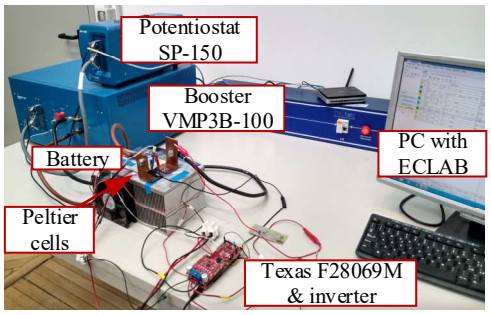

Fig. 3. Test setup

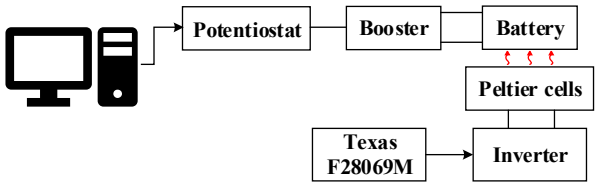

Fig. 4. Scheme of the test setup

The test procedure was divided into two steps: the internal resistance measurement phase and the cycle aging phase. The evaluation of the resistance was performed using GEIS at the beginning of the battery life and after each cycle aging phase.

A. Resistance measurement phase

The resistance of the LiB cell was measured at five different SOC levels (100%, 75%, 50%, 25%, and 0%) and eight different temperatures: 20 °C, 22.5 °C, 25 °C, 27.5 °C, 30 °C, 33.5 °C, 38 °C, and 46 °C directly from the booster,

which has an accuracy class on the impedance measurement defined as 1% of the reading.

The LiB cell was charged up to 100% of SOC using the constant current-constant voltage (CC-CV) protocol. This protocol involved charging the LiB cell at 10 A (1C) until the maximum cut-off voltage was reached. Then, a constant voltage of 4.2 V was applied until the current decayed to 100 mA (0.01C). After completing the charging process, the LiB cell was left to rest for 1 hour, and a GEIS from 10 kHz to 100 mHz was performed. After that, the LiB cell was discharged at 10 A (1C) until 75% of SOC was reached. After 1 hour of rest, another GEIS was performed. The same procedure was repeated, decreasing the SOC level by 25% each time until reaching 0% of SOC. Then, the temperature was changed, and the LiB cell was recharged using the CC-CV protocol to perform the same procedure at all the abovementioned temperatures.

B. Cycle aging phase

The cycle aging phase was performed at a constant temperature of 30 °C and consisted of a sequence of charging and discharging current steps. To speed up the cycle aging phase, these charging and discharging steps were performed at 50 A (5C) since, under constant temperature conditions, the current amplitude does not significantly affect battery aging [20]. After moving 10000 Ah, the charging and discharging steps were reduced to 40 A (4C) to avoid high frequency aging effects [25] caused by capacity fade. Nonetheless, the charging and discharging cycles were constrained by two boundaries: the voltage was limited between 3.45 V and 4.05 V, and the SOC was maintained between 20% and 80%. It is worth noting that, if the voltage boundaries were reached before, the charge moved in a cycle would be less than 60% of the capacity. However, according to [6], the shape of the aging cycle does not influence the aging process. Each cycle aging phase moved about 5000 Ah.

IV. Model Description

Neural networks (NN) are universal approximators and can estimate any nonlinear function with the required accuracy [26]. Indeed, in recent years NNs have been shown to solve complex non-linear problems [27], and have been extensively used in many different fields, such as computer sciences, finance, engineering, etc. (see, e.g., [28] and references therein). Compared with other ML modeling approaches, NNs have advantages in predicting an output without the knowledge of the exact analytic information of the modeled system. Another major benefit of NNs is their computational efficiency [28]. For all these reasons this work specifically focuses on NNs, due to their potential to effectively tackle highly nonlinear complex problems, with limited computational cost.

It is worth mentioning that other ML models (specifically, Support Vector Machines, LASSO/Ridge regression with polynomial features, Gradient Boosting Regressor, and Random Forests regressor) were tested and trained for the same task. However, preliminary results indicated that the NN approach outperformed the other models in both accuracy and computational time.

This Section is organized as follows: Section IV-A describes the process of building, training, and evaluating a suitable network model for the task at hand; Section IV-B explores Ensemble Learning, an ML technique that enables the combination of multiple simple learning models, such as the one built in Section IV-A, into a more robust aggregate model.

A. Neural Network Architecture

The main challenge in creating an appropriate NN model for the task of interest was the small size of the dataset, both in terms of the number of samples (160 samples for training purposes, 40 for testing), and feature size (3 features only: T, SOC, and moved charge).

A standard K-fold cross-validation approach was employed to train NN architectures, with $K = 4$ (i.e., the size of each fold equal to 40), with folds generated uniformly at random. Preliminary experiments were conducted using different feedforward networks with 2 or 3 hidden layers, each layer composed of 10 neurons at most. All these preliminary experiments, performed with different model configurations, showed a huge level of overfitting on the validation set, mostly due to the limited size of the overall dataset.

The need to prevent overfitting led to the final design of a small and compact network architecture, better suited to the limited complexity of the dataset. The employed network architecture was composed of a single dense layer composed of 5 neurons, activated by the softmax function. All neurons of the hidden layer were connected to a single output unit with no activation function (indeed, activation functions in the output of a NN are not needed for regression tasks). Nevertheless, ReLU and LeakyReLU were tested as output activation functions, but they provided worse results compared to not having an activation function at all. Standard choices such as: i) Mean Squared Error (MSE) as cost function, ii) Adam as an optimizer, and iii) batches of size 32 samples, were found to perform well and were selected for the final configuration. Finally, after some tuning, an initial learning rate of $5 \cdot 10^{-3}$ was chosen. The network architecture was trained for 2500 epochs in each experiment, and the weight configuration that achieved the best performance on the validation set was stored as the final model. The NN model employed in the experiments is summarized in TABLE II.

TABLE II. NN Architecture

Number of layers	2
Number of units in the hidden layer	5
Number of units in the output layer	1
Activation function of the hidden units	softmax
Activation function of the output unit	None
Loss function	MSE
Optimizer	Adam
Initial learning rate	$5 \cdot 10^{-3}$
Batch size	32

B. Ensembles

The compact NN model described in the previous section can be efficiently used as a building block of a more complex architecture. Based on this idea, it was decided to further enhance and refine the predictions of the network model through an Ensemble Learning technique, specifically by performing *bagging* (short for bootstrap aggregating) [29].

Bagging, in simple terms, is an ML method where the prediction output of an ML task is obtained by aggregating the predictions of multiple independent ML models. More

specifically, according to the bagging procedure, the original training set is sampled with replacement N times, $N > 1$, to obtain N training sets from the original one, sufficiently different from each other. Each training set is then used to train an ML model. During the prediction step, the output predictions of each one of the N independent ML models are aggregated with the predictions of all the other models, thus generating a single final result.

For a regression task, as the one presented in this work, aggregating the outputs of N ML models translates into averaging the output prediction of each model. Bagging is nowadays an established ML technique that reduces variance and mitigates overfitting, thus increasing prediction stability and accuracy [30].

Due to the limited size of the dataset and the compactness of the networks described in the previous section, it was decided to perform bagging with a large number of predictors, specifically $N = 100$ NNs. For each NN, a different training set was generated by sampling 160 samples with replacement from the original 160 samples. Statistically, this procedure implies that approximately 37% of instances are not sampled for each predictor, leaving them available as validation sets. The overall bagging procedure is illustrated in Fig. 5.

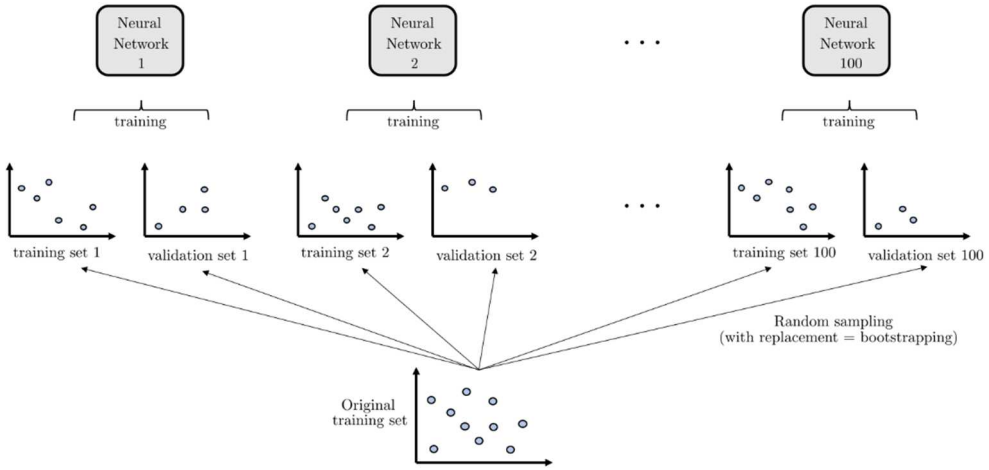

Fig. 5. Bagging architecture

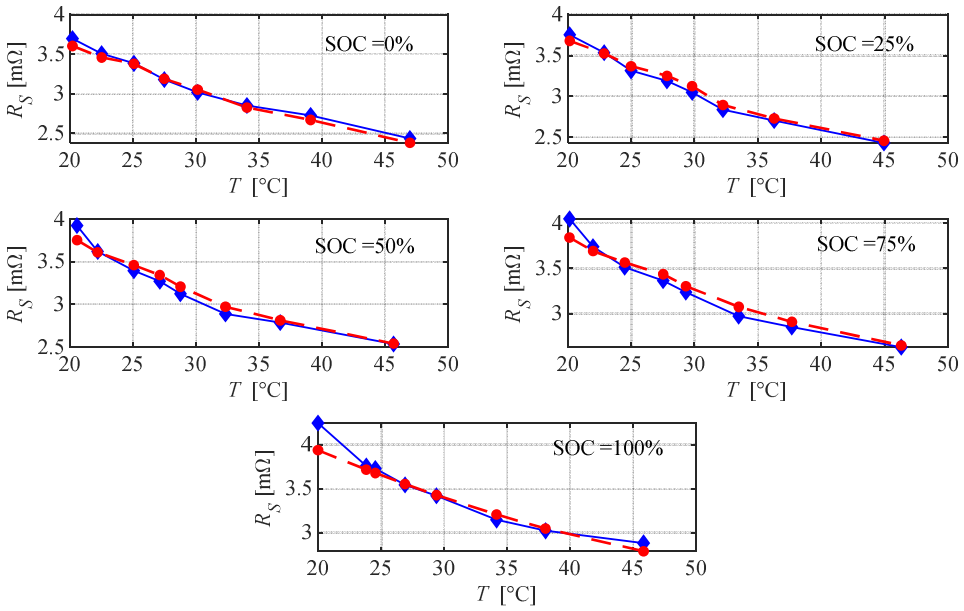

Fig. 6. Measured resistance (blu continuous lines) vs estimated value (red dashed lines)

V. Model Performances

All the experiments were run on the CPU of an AMD EPYC 7742 server, with a base processor speed of 2.25 GHz, 256 MB L3 cache, and no GPUs. Python was used as a programming language, with the Tensorflow library for the ML procedures.

The dataset used to train the model was composed of the experimental results obtained at all SOC levels and all aging levels, except the last one at 20 kAh. This model was then used to predict the resistance trend as a function of temperature when the moved charge is 20 kAh. Then, the results were compared with the experimental data obtained from the GEIS, as explained in Section III. The comparison of the two trends is depicted in Fig. 6. As can be seen from

the figures, the predicted resistance closely matches the measured value, especially at lower SOC levels.

The model performances can be evaluated by employing the relative error for a given temperature and SOC. Therefore, it is defined as:

$$\varepsilon(\mathrm{SOC},\mathrm{T}) = \frac{R_{S,e}(\mathrm{SOC},\mathrm{T}) - R_{S,m}(\mathrm{SOC},\mathrm{T})}{R_{S,m}(\mathrm{SOC},\mathrm{T})} \quad (1)$$

where $R_{S,e}$ is the estimated resistance value from the NN, while $R_{S,m}$ is the actual measured one. Once having computed the relative error, its statistical behavior can be evaluated. In particular, its average value is equal to -0.05%, while the 95th percentile value is between -4.5% and +2.5%. This is a remarkable performance, considering the limited value of the resistance that has to be measured and the class of the impedance measurement device which is equal to 1%.

The accuracy of predicting the battery resistance against temperature, $R_S(T)$, for each SOC, can be evaluated using the normalized root mean square error (NRMSE), which is defined as:

$$\mathrm{NRMSE}(\mathrm{SOC}) = \sqrt{\frac{\sum_T \left(R_{S,m}(T) - R_{S,e}(T)\right)^2}{\sum_T \left(R_{S,e}(T)\right)^2}} \quad (2)$$

The results are shown in Fig. 7.

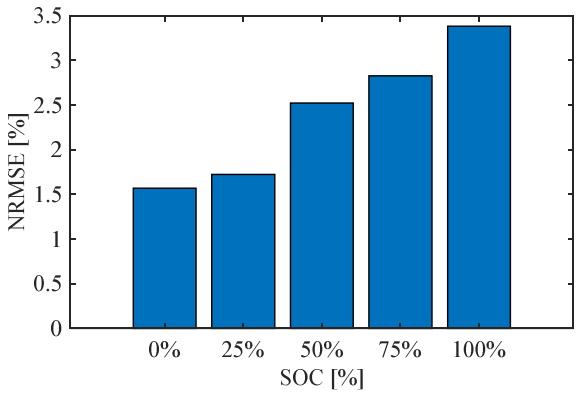

Fig. 7. NRMSE of $R_S(T)$ prediction when Q=20 Ah

The trend confirms the remarkable performance of the prediction for low SOC levels: when the SOC equals 0%, its value is reduced to 1.5%, while the model seems to behave worse at 100% of SOC, where the NRMSE doubles. This is mostly given by the inaccurate prediction of the resistance at low temperatures, specifically at $T = 20$ °C. The reason behind this lies in the different derivatives of the resistance in that region. Increasing the number of observations will easily reduce the prediction error. By neglecting that point, the NRMSE lowers to less than 2% and the 95th percentile of the relative error is reduced to about ±2%.

After evaluating the prediction of the resistance trend for a given aging condition, the model was trained to determine the value of $R_S(T)$ for each aging at a specified SOC. This means that the NN is able to reconstruct $R_S(T)$ correctly in each aging condition, even in an unknown SOC. To achieve this, the NN was trained using the entire dataset except for the experimental data at SOC = 0%. It was then asked with predicting the behavior of $R_S(T)$ at that specified SOC. As an example, the results of predicting the behavior when SOC = 0% are reported in Fig. 8.

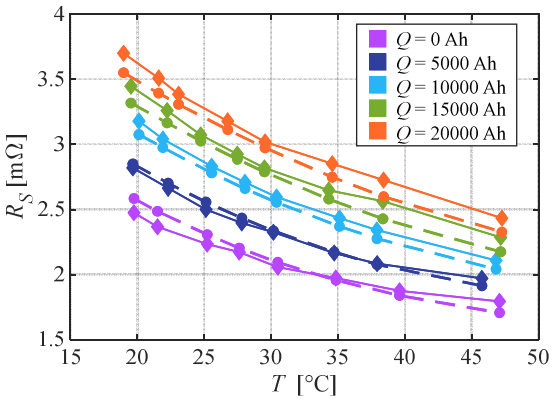

Fig. 8. Measured resistance (continuous lines) vs estimated value (dotted lines)

Also in this case, the NN performs quite well in estimating the $R_S(T)$ curves for the unknown SOC, with a relative error between -4% and +5% for the 95th percentile of observations, and a mean value of 1.4%. Additionally, the NRMSE value varies from 1.5% (for the blue curve of Fig. 8, namely Q=5 kAh) to 3.5% (when the battery is new). The results of NRMSE are reported in Fig. 9.

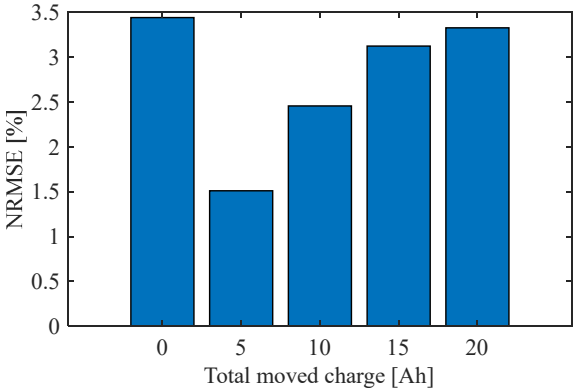

Fig. 9. NRMSE of $R_S(T)$ prediction when SOC=0%.

VI. Conclusion

Nowadays, the use of LiBs is spreading for manyfold applications, ranging from electronic devices to power grid-based applications. Despite their widespread adoption, their behavior is not yet fully understood to their inherent physical complexity. One of the key points of the research activity is the estimation of battery degradation and end of life. This work proposes a machine learning method applied to LiBs for estimating the behavior of internal resistance as a function of temperature, state of charge, and total moved charge, which can be a useful indicator for the state of health prediction.

The results show a good agreement between the predicted and experimental data, both for predicting the last aging level at each SOC and for predicting resistances at 0% of SOC for all aging levels. In both cases, the NN was trained using all the available complementary data. The 95th percentile of the relative error is below 5% and the NRMSE is below 3.5% for both cases. These results are noteworthy, especially considering the limited range of resistance to be measured and the class of the impedance measurement device set at 1%.

Moreover, the results can be further improved by expanding the size of the training dataset.

REFERENCES

[1] H. Deng and K. E. Aifantis, "Applications of Lithium Batteries," in *Rechargeable Ion Batteries*, Wiley, 2023, pp. 83–103. doi: 10.1002/9783527836703.ch4.

[2] I. Bloom *et al.*, "An accelerated calendar and cycle life study of Li-ion cells," *J. Power Sources*, vol. 101, no. 2, pp. 238–247, Oct. 2001, doi: 10.1016/S0378-7753(01)00783-2.

[3] R. . Wright *et al.*, "Calendar- and cycle-life studies of advanced technology development program generation 1 lithium-ion batteries," *J. Power Sources*, vol. 110, no. 2, pp. 445–470, Aug. 2002, doi: 10.1016/S0378-7753(02)00210-0.

[4] K. Nunotani *et al.*, "Development and performance evaluation of lithium iron phosphate battery with superior rapid charging performance - Second report: Evaluation of battery capacity loss characteristics," in *2011 IEEE Vehicle Power and Propulsion Conference*, IEEE, Sep. 2011, pp. 1–4. doi: 10.1109/VPPC.2011.6042998.

[5] S. S. Choi and H. S. Lim, "Factors that affect cycle-life and possible degradation mechanisms of a Li-ion cell based on LiCoO2," *J. Power Sources*, vol. 111, no. 1, pp. 130–136, Sep. 2002, doi: 10.1016/S0378-7753(02)00305-1.

[6] S. Barcellona, M. Brenna, F. Foiadelli, M. Longo, and L. Piegari, "Analysis of Ageing Effect on Li-Polymer Batteries," *Sci. World J.*, vol. 2015, pp. 1–8, 2015, doi: 10.1155/2015/979321.

[7] K. Asakura, M. Shimomura, and T. Shodai, "Study of life evaluation methods for Li-ion batteries for backup applications," *J. Power Sources*, vol. 119–121, pp. 902–905, Jun. 2003, doi: 10.1016/S0378-7753(03)00208-8.

[8] B. V. Ratnakumar, M. C. Smart, L. D. Whitcanack, and R. C. Ewell, "The impedance characteristics of Mars Exploration Rover Li-ion batteries," *J. Power Sources*, vol. 159, no. 2, pp. 1428–1439, Sep. 2006, doi: 10.1016/j.jpowsour.2005.11.085.

[9] S. Hossain, X. Kang, and S. Shrestha, "Effects of Temperature on Internal Resistances of Lithium-Ion Batteries," *J. Energy Resour. Technol.*, vol. 137, p. 31901, May 2015, doi: 10.1115/1.4028698.

[10] T. Momma, M. Matsunaga, D. Mukoyama, and T. Osaka, "Ac impedance analysis of lithium ion battery under temperature control," *J. Power Sources*, vol. 216, pp. 304–307, 2012, doi: https://doi.org/10.1016/j.jpowsour.2012.05.095.

[11] Y. Bao, W. Dong, and D. Wang, "Online Internal Resistance Measurement Application in Lithium Ion Battery Capacity and State of Charge Estimation," *Energies* , vol. 11, no. 5. 2018. doi: 10.3390/en11051073.

[12] D. Anseán, V. M. García, M. González, J. C. Viera, C. Blanco, and J. L. Antuña, "DC internal resistance during charge: Analysis and study on LiFePO<inf>4</inf> batteries," in *2013 World Electric Vehicle Symposium and Exhibition (EVS27)*, 2013, pp. 1–11. doi: 10.1109/EVS.2013.6914746.

[13] M. Ecker *et al.*, "Development of a lifetime prediction model for lithium-ion batteries based on extended accelerated aging test data," *J. Power Sources*, vol. 215, pp. 248–257, Oct. 2012, doi: 10.1016/j.jpowsour.2012.05.012.

[14] D.-I. Stroe, M. Swierczynski, S. K. Kar, and R. Teodorescu, "Degradation Behavior of Lithium-Ion Batteries During Calendar Ageing—The Case of the Internal Resistance Increase," *IEEE Trans. Ind. Appl.*, vol. 54, no. 1, pp. 517–525, Jan. 2018, doi: 10.1109/TIA.2017.2756026.

[15] S. Barcellona, S. Colnago, G. Dotelli, S. Latorrata, and L. Piegari, "Aging effect on the variation of Li-ion battery resistance as function of temperature and state of charge," *J. Energy Storage*, vol. 50, p. 104658, Jun. 2022, doi: 10.1016/j.est.2022.104658.

[16] H. Rauf, M. Khalid, and N. Arshad, "Machine learning in state of health and remaining useful life estimation: Theoretical and technological development in battery degradation modelling," *Renew. Sustain. Energy Rev.*, vol. 156, p. 111903, Mar. 2022, doi: 10.1016/j.rser.2021.111903.

[17] D. Roman, S. Saxena, V. Robu, M. Pecht, and D. Flynn, "Machine learning pipeline for battery state-of-health estimation," *Nat. Mach. Intell.*, vol. 3, no. 5, pp. 447–456, Apr. 2021, doi: 10.1038/s42256-021-00312-3.

[18] M. Brenna, F. Foiadelli, M. Longo, S. Barcellona, and L. Piegari, "Lithium-ion battery: A simplified modeling procedure and system simulation," in *2016 International Symposium on Power Electronics, Electrical Drives, Automation and Motion (SPEEDAM)*, IEEE, Jun. 2016, pp. 1034–1040. doi: 10.1109/SPEEDAM.2016.7525915.

[19] S. Barcellona, S. Colnago, P. Montrasio, and L. Piegari, "Integrated Electro-Thermal Model for Li-Ion Battery Packs," *Electronics*, vol. 11, no. 10, p. 1537, May 2022, doi: 10.3390/electronics11101537.

[20] S. Barcellona and L. Piegari, "Effect of current on cycle aging of lithium ion batteries," *J. Energy Storage*, vol. 29, p. 101310, Jun. 2020, doi: 10.1016/j.est.2020.101310.

[21] S. Barcellona and L. Piegari, "Lithium Ion Battery Models and Parameter Identification Techniques," *Energies*, vol. 10, no. 12, p. 2007, Dec. 2017, doi: 10.3390/en10122007.

[22] V. A. Agubra and J. W. Fergus, "The formation and stability of the solid electrolyte interface on the graphite anode," *J. Power Sources*, vol. 268, pp. 153–162, Dec. 2014, doi: 10.1016/j.jpowsour.2014.06.024.

[23] J. Li, E. Murphy, J. Winnick, and P. . Kohl, "Studies on the cycle life of commercial lithium ion batteries during rapid charge–discharge cycling," *J. Power Sources*, vol. 102, no. 1–2, pp. 294–301, Dec. 2001, doi: 10.1016/S0378-7753(01)00821-7.

[24] G. Ning, B. Haran, and B. N. Popov, "Capacity fade study of lithium-ion batteries cycled at high discharge rates," *J. Power Sources*, vol. 117, no. 1–2, pp. 160–169, May 2003, doi: 10.1016/S0378-7753(03)00029-6.

[25] M. Uno and K. Tanaka, "Influence of High-Frequency Charge–Discharge Cycling Induced by Cell Voltage Equalizers on the Life Performance of Lithium-Ion Cells," *IEEE Trans. Veh. Technol.*, vol. 60, no. 4, pp. 1505–1515, May 2011, doi: 10.1109/TVT.2011.2127500.

[26] S. Haykin, *Neural Networks: A Comprehensive Foundation*, 2nd ed. Prentice Hall PTR, 1998.

[27] D. Silver *et al.*, "Mastering the game of Go with deep neural networks and tree search," *Nature*, vol. 529, no. 7587, pp. 484–489, Jan. 2016, doi: 10.1038/nature16961.

[28] M. Capra, B. Bussolino, A. Marchisio, G. Masera, M. Martina, and M. Shafique, "Hardware and Software Optimizations for Accelerating Deep Neural Networks: Survey of Current Trends, Challenges, and the Road Ahead," *IEEE Access*, vol. 8, pp. 225134–225180, 2020, doi: 10.1109/ACCESS.2020.3039858.

[29] L. Breiman, "Bagging predictors," *Mach. Learn.*, vol. 24, no. 2, pp. 123–140, Aug. 1996, doi: 10.1007/BF00058655.

[30] P. Bühlmann and B. Yu, "Analyzing bagging," *Ann. Stat.*, vol. 30, no. 4, Aug. 2002, doi: 10.1214/aos/1031689014.